E-ISSN: 2664-6773
P-ISSN: 2664-6765
Impact Factor: RJIF 5.6
IJCBS 2023; 5(1): 12-17
www.chemicaljournal.org
Received: 11-11-2022
Accepted: 14-12-2022

Ammar S Mohammed
College of Agriculture Al-Hawija, University of Kirkuk, Iraq

Corresponding Author:
Ammar S Mohammed
College of Agriculture Al-Hawija, University of Kirkuk, Iraq

A novel three-step for the synthesis of organic reduced graphene oxide nanosheets as a water-soluble material with high electrical conductivity

Ammar S Mohammed

DOI: https://doi.org/10.33545/26646765.2023.v5.i1a.53

Abstract
This article has developed a novel procedure consisting of three stages to guarantee the production of a very conductivity and liquid rGO. It has been demonstrated that synthesizing aqueous systems of isolated, sparsely sulfonated graphene may be done easily and within specific requirements. It is helpful to imagine graphene, also known as rGO, to be among the most apparent graphene research results in opportunities for large-scale manufacturing and commerce. Whereas graphite may be easily oxidized and exfoliated in agitated environments to produce rGO, the size of such sheets is often constrained by breakage across fault lines throughout these processes. Various methods of characterization, such as XRD, FE-SEM, Raman, UV–vis, and FTIR, were utilized in order to carry out a comprehensive analysis and inspection of the rGO that had been synthesized.

Keywords: Graphene, rGO, electrical, synthesis

1. Introduction
The most recent description of this substance calls it "the lightest substance in human cosmos." Graphene, which consists of hexagonal shapes arranged sp^2-bonded carbon molecules in a hexagonal pattern arranged sheet, holds the potential for various uses, ranging from synthetic structures to quantum dots [1, 2]. However, as in other recently found forms of carbon (fullerenes and single-wall nanotubes), the rate-limiting steps in examining putative uses of graphene will determine how readily available the material is and how readily available it is easy it can be processed. For graphene, the availability of the material is hindered by the fact that it is necessary to overcome the high cohesive van der Waals energy (5.9 kJ mol-1 carbon) that is required to adhere graphitic sheets to one another. Starting with oxidized graphite, we offer a process that is both straightforward and amenable to scaling up for the production of aqueous systems of the isolated, thinly sulfated graphene surface. The fact that continuous graphene films formed by evaporation of an aqueous solution have a measurable electrical conductivity suggests that the broad, interconnected sp^2 carbon chain is reestablished in water-soluble graphene [3-5]. In the beginning, graphene was extracted by a process called physical exfoliating. This involves peeling off the upper layer of the pyrolysis process of graphite rock formations in order to collect the graphene. However, this technique is not appropriate for use on a wide scale. More recently, individual sheets of carbon nanotubes were thermally transformed to graphite after deposition on such a silicon substrate [9, 10]. This is another example of a technique that is best suited for use in a restricted range of applications. One method to get (specific job role) graphene oxide in bulk is to acquire it by exfoliating graphite that has been oxidized with strong acids, either through fast temperature increases or ultrasonic dispersal. The oxidation chemistry is very similar to the chemistry which is used to improve the properties of single-wall carbon nanotubes (SWNTs). This chemistry produces a range of oxygen functional groups (sOH, sOs, and sCOOH) largely at "fault" sites on the extremities of the SWNTs. In the presence of oxidizing chemicals with an adequate level of strength, functionalized flaws were also produced on the SWNT wall surfaces [6-8]. Since graphene oxide made from oxidized graphite involves important oxygen functionality and flaws, correcting the affiliated crystal structures perturbations brought on by oxidation is necessary to restore graphene's distinctive properties regardless of the laser ablation mechanics. With "ferric oxide chemistry," such as treating graphene and ammonia, these disturbances can be very briefly reduced, but the resultant materials are not likely to retain graphene's electrical

properties due to the remaining (passivated) flaws [9]. In an ideal scenario, graphene oxide must be severely decreased following exfoliating in order to regain the qualities that make graphene so appealing. In order to accomplish this goal, poly (n "graphitic related terms" were created by reducing highly porous graphite oxide in the vicinity of poly (sodium-4 styrene sulfonate), which resulted in the production of fascinating synthetic structures. However, depending on the requirements, having a polymeric dispersal agent present in graphene composites may not be desired. Highly porous graphite can be reduced in ammonium to produce graphite nanosheets, although these nanosheets have a low solubility in water (less than 0.5 mg/mL). By reducing graphite oxide in two phases, we propose a chemical pathway that can be followed to get soluble salts of separated graphene sheets. Through the utilization of our technology, residual oxide functionality is eliminated, and a regulated introduction of sulfonic acid is made in partially reduced graphene oxide. After the final version of the graphite, the presence of the charging sSO3units prevents the nanocrystalline sheets from clumping in the liquid, which results in the production of separated sheets of weakly sulfated graphene that have better water solubility [10, 11]. As a beginning material for the manufacture of graphene, we make use of graphite oxide, which is created by oxidizing graphite using acid. The oxidized result has a layered architecture similar to that of graphite. On the interior of stratified stacks of graphene oxide, -OH and >O functionalities break the graphene sheets' basal planes, while -COOH and hydroxyl group adorn the perimeter of the aircraft. In direct proportion to this, graphite oxide has a higher inter-layer design (from 0.34 nm in graphite to >0.6 nm in graphite oxide). Therefore, the van der Waals forces holding the layers together will weaken sonication, making a more effective exfoliation method. The highly functionalized graphene oxide produced as a result can produce stable dispersions in water. On the other hand, if the oxygen functionality is eliminated in order to produce graphene, the graphene reduces its capacity to be dispersed in water, and they begin to aggregate and ultimately hasten. Before the graphene oxide is completely reduced, we insert a sensible amount of p-phenyl-SO3H groups into it. This ensures that the resultant graphene is not agglomerated and that it is still water-soluble [12-14]. In this work, to assure the manufacture of a high conductivity and water-soluble rGO, a three-step process that includes sulfonation treatments with sulfuric acid has been proposed. A comprehensive electrical properties study of reduced graphene oxide was tackled in this article.

2. Theoretical overview of reduced graphene oxide (rGO)

2.1 Investigations of rGO

Andre Geim and Konstantin Novoselov were the first people to manufacture graphene in the year 2004 successfully. Their accomplishment has proven that graphene possesses a two-dimensional honeycomb-like lattice structure and that this structure is made up of a single sheet of sp^2-bonded carbon atoms. It was an important step forward since it was the first time that credible data was presented to back up the long-standing notion of graphene, which dates back to 1947. Because of its extraordinary electrical, mechanical, and chemical qualities, graphene has captured the interest of the scientific world ever since it was first synthesized. Graphene is an active material for gas sensing because of its enormous surface area, high carrier mobility, and high specific surface area ratio [15-17].

2.2 Notable properties and applications of the rGO

2.2.1 Electrical properties

With a conductance of 106 S/m and a sheet resistance of 31 /sq, graphene is the most highly conductive substance that may exist at room temperature. This is because graphene possesses very high electron mobility, 2 x 105 cm^2/Vs. There is a little overlap in graphene between the valence and conduction bands. As a consequence of this property, it is categorized as a semimetal and a semiconductor with minimal bandgap. Graphene is classified as a semi-metallic material given the presence of a certain concentration of exciton and holes in the valence band, even at temperatures as low as zero (while considering its gapless electronic structure, which means that electrons can swoop thru the bandgap). This is the source of graphene's good conductivity. Graphene possesses high electrical properties even at temperatures as low as absolute zero. When compared to a few layers of graphene, the electrical conductivity of a thin layer of graphene is approximately 10,000 times greater [19, 20].

2.3.2 Mechanical properties

Graphene is a substance that has a planar weight of 0.77 mg/m^2, making it an incredibly lightweight substance. In addition to this, its crystal structure is the most durable and abrasion-resistant of any known material. In comparison, the elastic modulus of the most popular type of steel is 200 GPa, whereas this material's structural rigidity is 125 GPa, and its elastic modulus is 1.1 TPA. With a breakage strength of 42 N/m, graphene possesses tensile stability that is one hundred times greater than that of steel. Graphene regions are prone to heat and mechanical variations in relative displacement, much like other materials. This is true for all types of substances. The frequently makes Euler illustrates that the magnitude of prolonged oscillations continuously increases over time with the magnitude of construction that is just double. As a result, the magnitude of these fluctuations would've been unbounded in frameworks of infinite size, despite the amplitude of such fluctuations being bounded in three-dimensional constructions (even in the limit of infinite size). This long-range difference in displacement has a negligible effect on the local deformation and elastic strain. It is widely held that, in the presence of externally supplied lateral force, a sufficiently big two-dimensional structure will, given enough time, fold and crumple into a shifting three-dimensional form. Ripples in hanging graphene sheets have been observed by scientists and has been speculated that the ripples are caused by thermal effects in the substance. As a direct consequence of this dynamical delamination, the topic of whether or not graphene is, in reality, a structure that only consists of two dimensions is still open for discussion. It was recently proved that all these reverberations, when amplified by the emergence of vacancy faults, can impart a deleterious Poisson's ratio into graphene, which results in the thinnest auxetic substance which has been found up to this moment. This was accomplished by creating the skinniest auxetic content possible. This was accomplished by creating the thinnest auxetic material possible. A plating procedure was used to include graphene nanomaterials into a nickel matrix to create Ni-graphene composites on a target substrate. The carbon nanosheets were deposited on the substrate. The increased contact between nickel and graphene and the avoidance of dislocation sliding in the nickel matrix brought about by graphene are responsible for the improvement in the mechanical features of the composites [20].

2.2.3 Optical properties

The one-of-a-kind optical characteristics of graphene provide a surprisingly high opacity for an atomic monolayer in a vacuum. Graphene absorbs 2.3 percent of all visible and invisible light. In this context, it denotes the fine-structure constant. This is a result of the "extraordinary minimal electron density of graphene sheets that highlights electron/hole conical artists meeting each other at the Dirac point... [which] is fundamentally different from far more popular quadratic huge bands." This is a direct result of the "unusual limited electron density of monolayer graphene." When calculating the optical permeability of graphite using the Fresnel equations in the thin-film limit, the Slonczewski–Weiss–McClure (SWMcC) band model of graphite predicts that the interparticle distance, hop value, and frequency will cancel out. Even though it was proven empirically, the measurement does not have a precision that allows it to improve upon other methods of estimating the fine-structure constant. The graphene films created via chemical vapor deposition (CVD) were characterized using a technique called cross plasmonic resonance, which measured the films' thickness and refractive index. The refractive index and the attenuation coefficient have been measured to have values of 3.135 and 0.897, respectively, at a length of 670 nm (6.7107 m) [21, 22].

The width was found to be 3.7 angstroms from a 0.5 mm^2 region, which agrees with the 3.35 angstroms recorded for the spacing between the layer-to-layer carbon atoms of graphite crystals. Graphene's reactions with organic and inorganic chemicals may be studied in real-time and without labels if the approach is utilized further. The presence of bidirectional plasmonic in non - reciprocal graphene-based gyrotropic surfaces has also been proven theoretically. This finding is related to the previous one. It is possible to continually tune the unidirectional operating frequency of graphene all the way from THz way up to near-infrared and even visible light if one effectively controls the chemical potential of graphene. Specifically, the horizontal frequency bandwidth in graphene can be one to two orders of magnitude higher than that in metal when both are subjected to the same magnetic field. This is made possible by graphene's exceptionally low good electron mass, which is an advantage over metal. By applying a voltage to the dual monolayer graphene ground transistor (FET) at ambient temperature, the band gap of graphene may be controlled from 0 to 0.25 eV (about 5 micrometers in length) [23-25]. When a magnetic field is introduced, the optical output of graphene may be tuned to operate in the terahertz range. Electrochromic behavior may be observed in graphene/graphene oxide complexes, which makes it possible to tune both ultrafast optical and linear characteristics. Its been established that a carbon material Goodfellow abrasion, also known as a one-dimensional photodetectors crystal, has been successfully imitated and that it is capable of exciting planar electromagnetic fields in the design.. This was accomplished by employing a 633 nm (6.33107 m) He–Ne laser as the light source. Graphene is a two-dimensional material composed of carbon atoms [26].

3. Experimental section

3.1 Synthesis of GO

A revised approach was used to make high GO based on Hummer's method. The improved procedure required pre-oxidizing graphite and adding additional potassium permanganate before quenching the reaction, as indicated below. In a mixture consisting of 10 grams of P_2O_5, 10 grams of $K_2S_2O_8$, and 100 milliliters of pure sulfuric acid, 4 grams of graphene were pre-oxidized over the course of 12 hours at 75 degrees Celsius with consistent stirring. The mixture was then cooled down in the refrigerator before being filtered, diluted with iced DDW, and washed with DDW until the pH was neutralized. This process was repeated until the mixture was finished. After that, the dark sample was subjected to overnight drying at a temperature of 50 ° C. The pre-oxidized GO was put into 100 ml of H_2SO_4 with 2 g of NaNO3, and the mixture was then frozen to 0 degrees Celsius in an ice bath. In order to keep the temperature from rising above 20 degrees Celsius, 12 grams of $KMnO_4$ were added very carefully. The reaction was agitated for a total of 12 hours while it was heated to 40 degrees Celsius. The reaction was stirred for almost a day and a half at a temperature of forty degrees Celsius after the addition of an additional 12 grams of KMnO4. After the reaction mixture had been cooled to room temperature, it was transferred to 600 milliliters of red-DDW and then cooled with 15 milliliters of hydrogen peroxide. The specimens were dried in hot air at 60 ° C. after being separated and disinfected five times with 400 ml of (30 percent HCl in DDW). The specimens were then washed with just enough DDW till the pH of both the rinse water was neutralized [27].

3.2 Synthesis of rGO

We presented a three-step process to achieve a high conductivity and moisture rGO preparedness: 1) hydrazine or before of graphene oxide; 2) sodium borohydride post-reduction, and 3) sulfonation treatment using concentrated sulfuric acid, accordingly. Just after the pH of the dispersion combination was dropped to 10 using a solution of 5 percent weight Na_2CO_3 in which was before the stage, it was customarily time to add 10 ml of hydroxy hydrate to the combination. The mixture contained 2 grams which were before GO and 1000 ml of DDW. After that, the reaction mixture was kept for six hours at a temperature of 90 degrees Celsius in a water bath with constant stirring. A transition from a dark brown to a black color was observed close to the end of this stage, which indicated the presence of aggregation. The partially recycled GO was agitated and then washed with water until the pH of the material was restored to its original value. After that, the partially rGO was s new in 1000 ml of DDW, and then 12 g of sodium borohydride was added to the mixture soon after the pH of the liquid was brought down to 10 using a suspension of 5 wt.% of sodium carbonate. The resulting mixture was then stirred consistently while being held in a water bath at a temperature of 90 degrees Celsius for a total of three hours. A number of gas bubbles were released, and it was observed that the mixture began to aggregate. The resulting black mixture was then given multiple washes with DDW before being allowed to dry. In the final step, the already-prepared rGO was re-dispersed in 400 ml of hydrochloric and kept at a temperature of 120 degrees Celsius with gentle stirring for a period of 12 hours. This was done to increase the stability of the compound and recover its coiled form.The solution was gently diluted with DDW after cooling to room temperature. Finally, the finished mixture was washed, washed completely with DDW, dry, and stored for future use [28].

3.3 Characterization

XRD diffraction patterns of PEDOT: PSS were obtained by utilizing a Brucker diffractometer (D8 Advance, Germany) in conjunction with a Cu K radiation source (= 1.54059)

operating at a power setting of 1600 w (40 kV,40 mA) in the 2theta range (5o-65o). In order to analyze the materials' absorption spectra, an IRAffinity-1S (Shimadzu, Japan) spectrophotometer was utilized to record FTIR spectra from a range of 4000 cm1 to 600 cm1 during the course of the experiment. The Raman spectra ranging from 200 cm-1 to 3000 cm-1 were obtained by employing a laser with a wavelength of 785 nm as the source of the excitation wavelength and a 100 mW XploRA PLUS confocal Raman microscope. The field-emission scanning electron microscopy was utilized to analyze the surface morphology of the samples (FESEM, Mira 3-XMU). The Jasco V-750 UV-Visible spectrophotometer was used to gather absorption spectra in the UV-visible region, extending from 190 to 900 nanometers.

4. Results and Discussion

X-ray diffraction was used to examine the crystallinity of pure GO and rGO. The XRD patterns and phase structures of both materials are shown in Figure 1. The formation of highly oxidized GO was demonstrated by the presence of a prominent peak at 2theta = 10.82 in the graphene oxide (GO) XRD pattern. This peak was ascribed to (001) graphene oxide. This diffraction peak has been right-shifted to 2theta = 25.3 inside the Xrd analysis of rGO due to the release of different oxygen-containing groups in the graphene structure. This has resulted in a contraction in the intercellular d-spacing of 3.52.

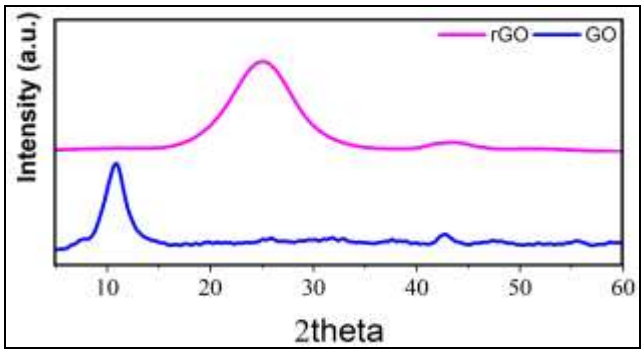

Fig 1: XRD pattern of GO and rGO

Figure 2 depicts the FT-IR spectrum of both of the samples collected from the experiment. The GO spectrum exhibits a series of strong absorption bands at the following wavelengths: 3410, 1720, 1620, and 1230 cm^{-1}. The stretch vibration modes of the carboxylic (vOH) groups or the leftover adsorption H_2O atoms are likely to blame for the broadband signal that is centered at 3410 cm^{-1}. The bent vibration of nucleophile water molecules may be responsible for a narrower band found at around 1720 cm_{-1} or the C = O stretching of the carboxyl group is responsible for this band. It is believed that the maximum that can be found at a frequency of 1620 cm_{-1} is caused by the stretching vibrations of C = C in the phenyl ring that originates from the unoxidized graphitic domain. The wave that may be observed at a frequency of 1230 cm_{-1} is caused by a bending vibration that occurs within the C–OH band of the alcohol molecule. It is believed that the group that was discovered at a frequency of 1050 cm_{-1} can be attributed to the symmetric stretching of the C–O bond that is present in the epoxy C–O–C complex. For instance, the infrared spectra of rGO indicate that there was a significant weakening of all ligands. This is suggested by the fact there's less energy in each spectrum. Only the absorption peaks that fall within the range of 1400–1800 cm^{-1} may still be observed [29, 30].

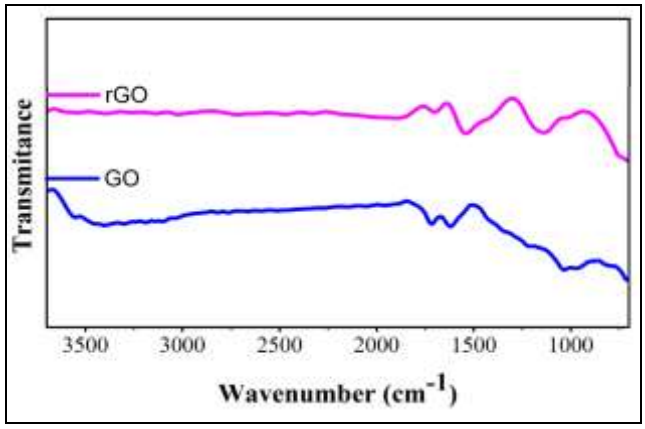

Fig 2: FTIR spectra of GO and rGO

Raman spectroscopy is an efficient method for determining the type of interaction that exists in a wide variety of carbon-based substances. As can be seen in Figure 3, Raman examinations were carried out on both graphene oxide (GO) and reduced graphene oxide (rGO) in order to describe sp^2 subdomains and confirm the architectural changes that occurred during the chemical reduction of GO to rGO. As a result of the oxygen of graphite and the o stretching mode of the C = C link present in the phenyl ring of GO in all commodities carbon atoms, the Raman spectra of GO showed the presence of a strong G band at 1594 cm^{-1}. This band was located at 1594 cm^{-1}. The strong oxidation D band at 1348 cm^{-1} suggests that the size of the in-plane sp^2 domains has shrunk, which may be owing to the hard oxidation process of GO causing deformities in the sp^2 domains, the development of defects, and vacancies. The D and G peaks, as shown by rGO, were located at 1329 cm^{-1} and 1575 cm^{-1}, respectively. As a result of the restoration of the carbon atoms' hexagonal network, the G band's location shifted to blue (in the direction of smaller wavenumbers), as measured concerning GO. Proof that the thermal decomposition affected the structure of GO so that it contains more flaws can be found in the fact that the Absorption bands in rGO have greater energy than it does in GO. The increment size of the sp^2 clusters is another component that may be contributing to the reduction in the full width at half-maximal of the D band. This is one possible explanation for the phenomenon. It is possible to determine an approximation of the typical size of the sp^2 cluster present in carbon materials by comparing the intensity of the ID and IG bonds. The D/G ratios of GO and rGO correlate to one another and are determined to be 0.94 and 1.2, respectively [31, 32].

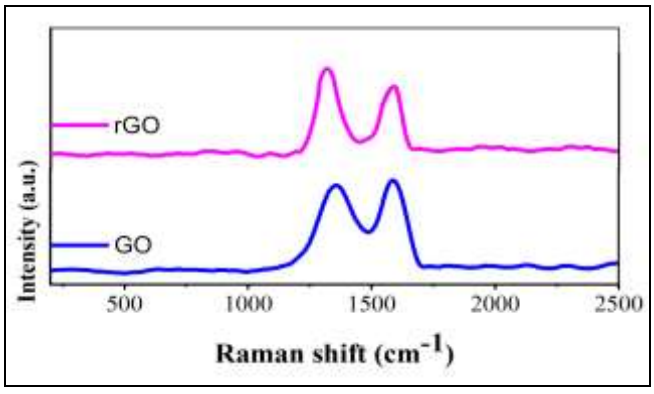

Fig 3: Raman Spectroscopy of GO and rGO

UV-vis spectroscopy was used to observe and record each step of the preparations for both GO and rGO. As seen in Figure 4, GO demonstrates a distinct absorption peak located at 225 nm. This peak is attributed to the –* transitions that occur in the C–C aromatic rings. After the conversion of GO into rGO, there was a discernible movement to the red of this absorption peak, which settled around 280 nm. The reinstatement of sp2 coupling in the GO sheets after a decrease causes a change in the conductivity and optical characteristics of rGO, which is responsible for the red shift in the spectroscopic analysis of reduced GO (rGO) [33].

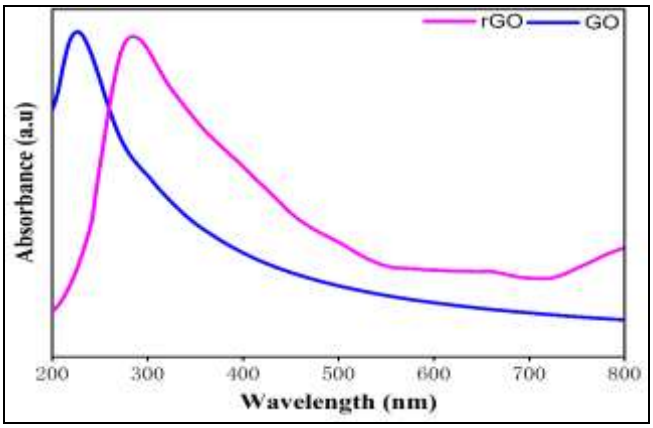

Fig 4: UV-vs spectra of GO and rGO

In order to investigate the surface characteristics of both GO and rGO, a technique known as field emission scanning electron microscopy (FE-SEM) was utilized. According to what was shown in Figure 5, the GO and rGO materials appear to be made up of thin sheets that have been crumpled and accumulated unevenly to form a fractured solid.

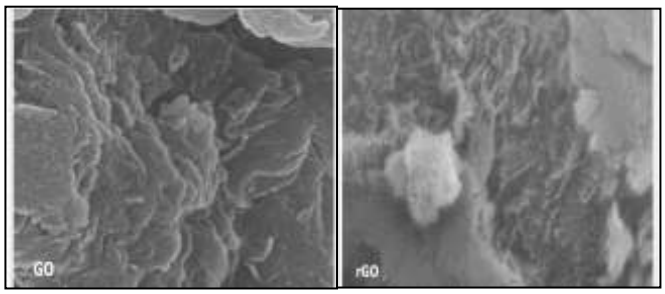

Fig 5: FE-SEM image of GO and rGO

5. Electrical conductivity analysis

The degree to which graphite has been converted to graphene may probably be estimated most accurately from the material's electrical conductivity. A water-soluble graphene layer that was dried to a thickness of fewer than three micrometers and comprised of graphite oxide, solubilized graphite oxide, and tungsten flakes was created on a glass slide. The film is dried at 120 °C Fahrenheit before measuring its electrical conductivity. The result provides information on the conductance of graphite, graphene, and solubilized carbon nanotubes (GO-SO3H). Because it does not possess an extensive-conjugated orbital system, graphite oxide does not possess conducive properties. Following prereduction, the conductivity of the GO- SO3H product is measured to be 17 S/m, which indicates that conjugation has been partially restored. Following the further reduction of GO-SO3H to graphene using hydrazine, the conductivity was found to have increased by more than 70 times, reaching 1250 S/m. In contrast, the conductivity of identically formed graphite flakes is only four times greater than that of a dried graphene layer when tested under the same circumstances (6120 S/m). The large conjugated sp2-carbon network is reinstated in the water-soluble graphene, which may be deduced from the fact that the electrical conductivity of the contiguous evaporating layer of nanomaterials is maintained. The friction coefficients are lower limits because the measurement includes contributions from both in-plane and through-plane electron conduct and percolate touch resistances in the evaporated layer. As a result, the conductivities are not exact values. In addition, the lateral dimensions of the graphite have been measured to be between 30 and 40 micrometers, which is a magnitude greater than the aspects of the water-soluble graphene. Measurements of this sort have been shown to affect the permeability that has been measured [34].

6. Conclusion

In conclusion, we have described a method that allows for isolating graphene that is soluble in water and can be manufactured in large quantities. The vast majority of oxygen-containing functional groups have been eliminated from our product. The electrical conductivity of the water-soluble graphite is equivalent to that of graphite. Single layers of graphite are what makeup diamond in its natural state. If more surface modifications are carried out, graphene that can be dissolved in alcohol might become available. This would further expedite the application of graphene in composites, particle emitters' displays, segments and sub tunable, circuits, and supersensitive chem detectors.

7. References

1. Chethan B, Prakash HR, Ravikiran YT, Vijayakumari SC, Ramana CV, Thomas S, *et al*. We are enhancing the humidity sensing performance of polyaniline/water-soluble graphene oxide composite. Talanta. 2019;196:337-344.
2. Jovanovic S, Haenssler OC, Budimir M, Kleut D, Prekodravac J, Markovic BT. Reduction of graphene oxide and graphene quantum dots using nascent hydrogen: The investigation of morphological and structural changes. Resolution and Discovery. 2020;5(1):1-4.
3. Jiang Z, Gao Y, He L, Song H, Zhou J, Zhu R. Helical edge states of topological photonic crystals with line defects. Applied Optics. 2019;58(9):2294-2299.
4. Barrutia L, Ochoa-Martínez E, Gabás M, Centeno A, Zurutuza A, Rey-Stolle I, *et al*. Evidence of Decreased Optical Absorption of Chemical Vapor Deposition Graphene Multilayers Deposited on Semiconductor Structures. ACS Photonics. 2022;9(3):868-872.
5. Bhagabati P, Rahaman M, Bhandari S, Roy I, Dey A, Gupta P, *et al*. Synthesis/preparation of carbon materials. In Carbon-Containing Polymer Composites. Springer, Singapore; c2019. p. 1-64.
6. Xu X, Huang J, Li J, Yan J, Qin J, Li Z. A graphene oxide-based AIE biosensor with high selectivity toward bovine serum albumin. Chemical Communications. 2011;47(45):12385-12387.
7. Watcharotone S, Dikin DA, Stankovich S, Piner R, Jung I, Dommett GH, *et al*. Graphene-silica composite thin films as transparent conductors. Nano letters. 2007;7(7):1888-1892.
8. Jung I, Pelton M, Piner R, Dikin DA, Stankovich S, Watcharotone S, *et al*. Simple approach for high-contrast

optical imaging and characterization of graphene-based sheets. Nano Letters. 2007;7(12):3569-3575.
9. Kuznetsova A, Popova I, Yates Jr JT, Bronikowski MJ, Huffman CB, Liu J, *et al*. Oxygen-containing functional groups on single-wall carbon nanotubes: NEXAFS and vibrational spectroscopic studies. Journal of the American Chemical Society. 2001;123(43):10699-10704.
10. Fedoseeva YV, Bulusheva LG, Koroteev VO, Mevellec JY, Senkovskiy BV, Flahaut E, *et al*. Preferred attachment of fluorine near oxygen-containing groups on the surface of double-walled carbon nanotubes. Applied Surface Science. 2020;504:144357.
11. Deline AR, Frank BP, Smith CL, Sigmon LR, Wallace AN, Gallagher MJ, *et al*. Influence of oxygen-containing functional groups on carbon nanotubes' environmental properties, transformations, and toxicity. Chemical reviews. 2020;120(20):11651-11697.
12. Gu W, Wei Y, Liu B, Hu L, Zhong L, Chen G. Polyacrylic Acid-Functionalized Graphene@ Ca (OH) 2 Nanocomposites for Mural Protection. ACS omega. 2022;7(14):12424-12429.
13. Abdelhalim AO, Sharoyko VV, Ageev SV, Farafonov VS, Nerukh DA, Postnov VN, *et al*. Graphene oxide of extra high oxidation: A wafer for loading guest molecules. The Journal of Physical Chemistry Letters. 2021;12(41):10015-10024.
14. Lowe SE, Shi G, Zhang Y, Qin J, Wang S, Uijtendaal A, *et al*. Scalable production of graphene oxide using a 3D-printed packed-bed electrochemical reactor with a boron-doped diamond electrode. ACS Applied Nano Materials. 2019;2(2):867-878.
15. Huang JY, Ding F, Yakobson BI, Lu P, Qi L, Li J *et al*. In situ observation of graphene sublimation and multi-layer edge reconstructions. Proceedings of the National Academy of Sciences. 2009;106(25):10103-10108.
16. Geim AK. Graphene prehistory. Physica Scripta. 2012;2012(T146):014003.
17. Vickers NJ. Animal communication: when i'm calling you, will you answer too?. Current biology. 2017;27(14):R713-R715.
18. Liang L, Wang J, Lin W, Sumpter BG, Meunier V, Pan M. Electronic bandgap and edge reconstruction in phosphorene materials. Nano letters. 2014;14(11):6400-6406.
19. Lu M, Ge Y, Wang J, Chen Z, Song Z, Xu J, *et al*. Ultrafast Growth of Highly Conductive Graphene Films by a Single Subsecond Pulse of Microwave. ACS nano, 2022;16(4):6676-6686.
20. Wintterlin J, Bocquet ML. Graphene on metal surfaces. Surface Science. 2009;603(10-12):1841-1852.
21. Soracco D. The Path to Graphene Synthesis and Applications; c2010.
22. Καλλιβωκάς Σ. Statistical and mechanical properties of graphene using Monte Carlo simulations (Doctoral dissertation); c2016.
23. Jussila H, Yang H, Granqvist N, Sun Z. Surface plasmon resonance for characterization of large-area atomic-layer graphene film. Optica. 2016;3(2):151-158.
24. Miao Y, Liu B, Zhang K, Liu Y, Zhang H. Temperature tunability of photonic crystal fiber filled with Fe 3 O 4 nanoparticle fluid. Applied Physics Letters. 2011;98(2):021103.
25. Nair RR, Blake P, Grigorenko AN, Novoselov KS, Booth TJ, Stauber T, *et al*. Universal dynamic conductivity and quantized visible opacity of suspended graphene. arXiv preprint. 2008;arXiv:0803-3718.
26. Sreekanth KV, Zeng S, Shang J, Yong KT, Yu T. Excitation of surface electromagnetic waves in a graphene-based Bragg grating. Scientific reports. 2008;2(1):1-7.
27. Pandey S. Highly sensitive and selective chemiresistor gas/vapor sensors based on polyaniline nanocomposite: A comprehensive review. Journal of Science: Advanced Materials and Devices. 2016;1(4):431-453.
28. Han MG, Foulger SH. Facile synthesis of poly (3, 4-ethylenedioxythiophene) nanofibers from an aqueous surfactant solution. Small. 2016;2(10):1164-1169.
29. Nguyen VC, Kheireddine S, Dandach A, Eternot M, Vu TT H, Essayem N. Acid Properties of GO and Reduced GO as Determined by Microcalorimetry, FTIR, and Kinetics of Cellulose Hydrolysis-Hydrogenolysis. Catalysts. 2016;10(12):1393.
30. Bui NQ, Mascunan P, Vu TTH, Fongarland P, Essayem N. Esterification of aqueous lactic acid solutions with ethanol using carbon solid acid catalysts: Amberlyst 15, sulfonated pyrolyzed wood and graphene oxide. Applied Catalysis A: General. 2018;552:184-191.
31. Stankovich S, Dikin DA, Piner RD, Kohlhaas KA, Kleinhammes A, Jia Y, *et al*. Synthesis of graphene-based nanosheets via chemical reduction of exfoliated graphite oxide. carbon, 2007;45(7):1558-1565.
32. Vickers NJ. Animal communication: when i'm calling you, will you answer too?. Current biology. 2017;27(14):R713-R715.
33. Martí M, Fabregat G, Estrany F, Alemán C, Armelin E. Nanostructured conducting polymer for dopamine detection. Journal of Materials Chemistry. 2010;20(47):10652-10660.
34. Watcharotone S, Dikin DA, Stankovich S, Piner R, Jung I, Dommett GH, *et al*. Graphene-silica composite thin films as transparent conductors. Nano letters. 2007;7(7):1888-1892.